CrystEngComm

Profoundly improved photostability of dimetronidazole by cocrystallization

Journal:	*CrystEngComm*
Manuscript ID	CE-ART-04-2022-000597.R2
Article Type:	Paper
Date Submitted by the Author:	31-Jul-2022
Complete List of Authors:	Hao, Xinghui; Hebei Agricultural University LI, Jinhui; Hebei Agricultural University Wang, Chenguang; Evelo Biosciences, Formulation Zhao, Xinghua; Hebei Agricultural University He, Xin; Hebei Agricultural University Sun, Changquan; University of Minnesota,

ARTICLE

Profoundly improved photostability of dimetronidazole by cocrystallization

Received 00th January 20xx,
Accepted 00th January 20xx

DOI: 10.1039/x0xx00000x

Xinghui Hao[#a,b], Jinhui Li[#a, c], Chenguang Wang[d], Xinghua Zhao [a,b], Xin He[a,b*] and Changquan Calvin Sun[*d]

Dimetronidazole (DMZ), an veterinary antibiotic, exhibits poor photostability with only 80.38% potency remaining after exposure to illuminance of 4500 lux for 7 days. The photodegradation is accompanied by obvious color change. A 1:1 cocrystal of DMZ with saccharine exhibited profoundly improved photostability with 98.95% of DMZ remaining after 7 days under the same light exposure. Thus, this new cocrystal can be used to develop more stable drug products of DMZ.

Introduction

Dimetronidazole (1,2-dimethyl-5-nitroimidazole, Scheme 1a, DMZ) [1] is an antibacterial and antiprotozoal veterinary drug for treating anaerobic and protozoal infections, e.g., chicken trichomonad,[2] bovine trichomoniasis, swine treponema hyodysenteriae and anaerobion.[3, 4] DMZ has been banned as a prophylactic veterinary drug in China, some EU countries, and some North American countries for safety reasons. However, it is still used in some countries, including Australia, Canada and Denmark, for treating infections in food animals.[5] In addition to accepted therapeutic efficacy, clinical resistance to nitroimidazole based drugs is known.[6] Low biodegradability, along with the relatively good aqueous solubility of DMZ (0.062 mol/L presumably at ambient temperature [7, 8] or 9.69 mg/mL at 20 °C[9]) lead to potential water pollution in the environment.[10] DMZ needs to be protected from light during storage because it degrades relatively quickly upon exposure to light, which usually leads to a color change.[11] Similar to other nitromidazoles drugs, such as metronidazole and tinidazole, the site of photodegradation of DMZ occurs at the nitrogen-containing imidazole ring,[12, 13] involving the conversion of the nitro group into a nitrite ester, which is then cleaved into oxyl and nitric oxide radicals (Scheme 1c).[11, 14] Thus, safer and more effective use of DMZ will clearly benefit from an improved photostability. Pharmaceutical cocrystals are homogeneous supra-molecules formed by non-covalent bonds, such as hydrogen bonds, π-π and *van der* Waals interactions, between active pharmaceutical ingredients (APIs) and cocrystal formers.[15, 16] The changes in molecular packing after cocrystallization affect the physicochemical properties of an API. For examples, cocrystallization has been used to change drug solubility,[17-20] bioavailability,[15, 21, 22] permeability,[23, 24] physical and chemical stability,[25-27], and taste.[23, 28] We note that not all changes are pharmaceutically favourable. For example, solubility may be decreased by cocrystallization.[23, 29, 30]

Except for DMZ, no crystal structures of other DMZ crystals have been reported in the Cambridge Structural Database (CSD). However, we were able to prepare a cocrystal of DMZ with saccharin (Scheme 1b), which opens the possibility of addressing the photostability issue of DMZ by crystal engineering to facilitate drug development.

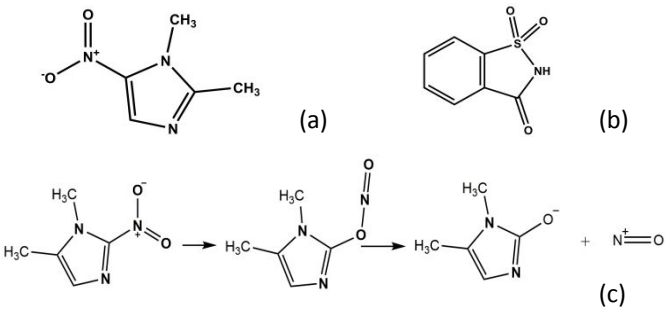

Scheme 1. Chemical structures of (a) dimetronidazole (DMZ), (b) saccharin (SAC), and (c) photo-degradation of DMZ.

Experimental section

Materials

Dimetronidazole (HPLC, 98.4% purity) was a gift from Baoding Jizhong Pharmaceutical Co., Ltd (Baoding, China). Saccharin ($C_7H_5O_3NS$) was purchased from Shanghai Aladdin Biochemical Science and Technologies Co., Ltd (Shanghai, China). All chemicals were used as received.

[a.] *College of Veterinary Medicine, Hebei Agricultural University, Baoding, Hebei 071000, China.*
[b.] *Veterinary Biological Technology Innovation Center of Hebei Province, Baoding, Hebei, 071000, China.*
[c.] *Hebei Shengxue Dacheng Pharmaceutical(Tangshan)Co., Ltd. 064000, China.*
[d.] *Pharmaceutical Materials Science and Engineering Laboratory, Department of Pharmaceutics, College of Pharmacy, University of Minnesota, Minneapolis, MN 55455, USA.*
† Electronic Supplementary Information (ESI) available. CCDC 2063120.
For ESI and crystallographic data in CIF or other electronic format see DOI: 10.1039/x0xx00000x

Dimetronidazole-Saccharin Cocrystal (DMZ-SAC, 1:1)

DMZ-SAC cocrystal was prepared using a slurry method. DMZ (38.5 mg, 0.27 mmol) and SAC (50.0 mg, 0.27 mmol) were suspended in 1 mL water at room temperature with a magnetic stirring bar at 200 rpm for 24 h. The solid was filtered and dried at 60 °C overnight.

Single crystals of DMZ-SAC were obtained by slow evaporation. DMZ (87.5 mg, 0.62 mmol) and SAC (113.6 mg, 0.62 mmol) were dissolved in about 10 mL water at 45 °C under stirring to obtain a clear solution, which was allowed to slowly evaporate on bench undisturbed. Transparent needle-like crystals were obtained after 5-7 days at room temperature.

X-ray diffraction analysis

Powder X-ray diffraction (PXRD) analysis were carried out using a TD-3700 X-ray diffractometer (Dandong, China) equipped with a one-dimensional array detector ($\lambda_{Cu\text{-}K\alpha}$ =1.54056 Å) operated at 30 kV and 20 mA. Powder samples were scanned between 5° and 35° (2θ) with 0.015 °step size and 0.1s/step scan speed. The instrument was calibrated using a silicon standard.

The single crystal X-ray diffraction data was collected at 150 K on an Agilent Technologies Gemini A Ultra system with graphite monochromated Cu K_α radiation (λ = 1.54178 Å). Cell refinement and data reduction were performed using the program CrysAlis^{PRO}. Crystal structure was solved by the direct method using the Olex2 program. Lattice parameters were refined by the full-matrix least-squares method on F^2. Non hydrogen atoms were refined using anisotropic displacement parameters, while all hydrogen atoms were placed in calculated positions with fixed isotropic thermal parameters.

Crystal lattice energy

The crystal structures were optimized using the COMPASS force field in the Forcite module of Materials Studio (v2019, Biovia Software Inc., San Diego, CA, USA) with associated charges and ultrafine quality selected. During the optimization, the molecules and crystal packing were allowed to relax, but the unit cell parameters were fixed. The "Ewald" electrostatic summation method and "atom based" *van der* Waals summation were chosen.

Intermolecular interaction energy

The pairwise intermolecular interaction energy (Table S1) was estimated using CrystalExplorer and Gaussian09 from experimental crystal geometry.[31, 32] Considering the uncertainty of hydrogen position by single crystal X-ray diffraction, hydrogen positions were normalized to standard neutron diffraction values before the calculation. The hydrogen positions were normalized to standard neutron diffraction values prior to calculation using the CE-B3LYP electron densities model. The total intermolecular interaction energy for a given pair of molecules is the sum of the electrostatic, polarization, dispersion, and exchange-repulsion components, with scale factors of 1.057, 0.740, 0.871, and 0.618, respectively. [33, 34]

Scanning electron microscopy (SEM)

Powder samples were distributed on glass slides with black double-sided adhesive carbon tape and sputtered with gold. Morphology of the samples was analyzed using a Hitachi S4800 scanning electronic microscopy (Hitachi, Japan) operating at 20 kV.

Fourier transform infra-red spectroscopy (FT-IR)

FT-IR spectra collected from 1% dispersion in KBr pellets were recorded in Nicolet iS5 FT-IR spectra (ThermoFisher, USA) for the samples. For each sample, a total of 64 scans were collected over the range of 4000 to 400 cm^{-1} with a resolution of 0.2 cm^{-1} for.

Thermogravimetric analysis (TGA) and Differential scanning calorimetry (DSC)

TGA profiles were collected on a SDT Q600 thermal analyzer (TA instrument, USA). DSC profiles were collected using a DSC 3 instrument (Mettler Toledo, Zurich, Switzerland). In both experiments, approximately 5 mg of each lightly grinded sample was loaded into an aluminium Tzero pan and heated from 25 °C to 400 °C at a heating rate of 10 °C/min under continuous nitrogen purge at 50 mL/min.

Hot stage microscope (HSM)

Morphology of cocrystal was observed under a polarized light-microscope (DM2700P, Leica, Germany), equipped with a hot-stage. Samples were heated from room temperature to 280 °C at a rate of 10 °C/min. The hot stage was controlled with a temperature controller (THMSG600, Linkam Scientific Instruments, Ltd., Waterfield, UK).

Photostability experiment

Approximately 1,000 mg of either DMZ or DMZ-SAC was spread on a glass petri dish, which was placed in a stability chamber (GXZ-430B, Ningbo, China) with an illuminance of 4500 lux at 25 °C and 15% RH. Approximately 100 mg of sample was collected every day and DMZ amount was determined by HPLC (Model 1525, Waters Corporation, Milford MA, USA).

Powder dissolution

For powder dissolution studies of DMZ and DMZ-SAC, each powder was milled and passed through standard sieves to obtain samples in 75~150 µm size range. 50 mL of deionized water was added to a beaker containing an excess amount of powder (about 1,500 mg) and stirred at 250 rpm. The temperature was maitained at 37 °C by a circulating water bath. 100 µL of the medium was withdrawn using a syringe at predetermined time points, filtered through a 0.22 µm nylon membrane, properly diluted, and then assayed by UV-Vis spectrophotometry at 320 nm.

Results and discussion

Powder X-ray diffraction

The PXRD patterns for DMZ, SAC and DMZ-SAC are shown in Fig. 1. The diffractogram of DMZ-SAC is distinct from DMZ, SAC, and their physical mixture (PM), where new diffraction peaks at 6.94°, 11.6°, 14.0°, 17.9° and 28.5° 2θ are observed while characteristic peaks of DMZ (12.9° and 18.7°) and SAC (9.5°, 15.9° and 20.0°) are absent. In addition, all the peaks in the experimental PXRD pattern closely match those in the pattern calculated from the single crystal structure of DMZ-SAC (Fig. 1e), confirming the phase identify of the DMZ-SAC cocrystal.

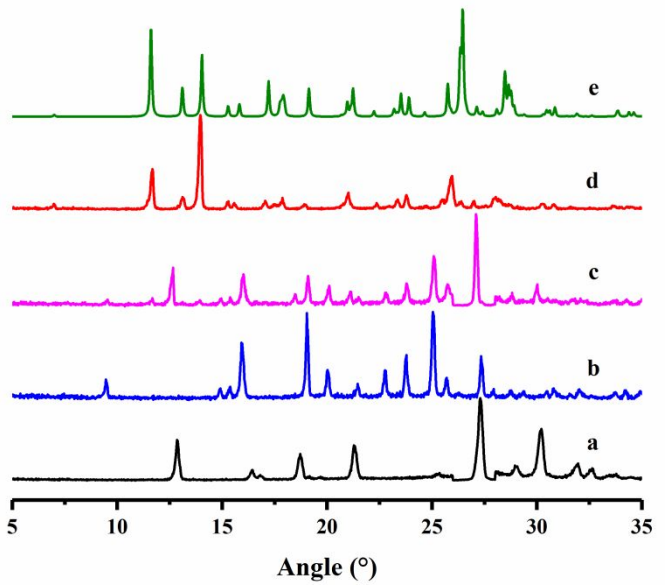

Fig. 1. X-ray powder diffraction patterns of a) DMZ, b) SAC, c) PM, d) experimental DMZ-SAC, and e) calculated DMZ-SAC. Normalized peak intensity is used.

Crystal structure

The crystal structure of DMZ-SAC (monoclinic, space group $P2_1/n$) revealed a 1:1 mole ratio of DMZ to SAC. DMZ and SAC form a heterodimer through a N-H···N hydrogen bond (2.739 Å) (Fig. 2a). Dimers stack along the *a-axis* to form a column, which is stabilized via the C-H···O=S (3.339 Å and 3.483 Å) weak hydrogen bonds. Within each column, the adjacent dimers differ in orientation by 180°. The columns are connected by C-H···O=C (2.935 Å) hydrogen bonds to form a 2D sheet along (002) plane (Fig. 2b). The 2D sheets stack to form a 3D structure, which is stabilized through C-H···O=N (3.214 Å and 3.478 Å) hydrogen bonds (Fig. 2c). Crystallographic data, structure and refinement details are given in Table 1.

Scanning Electron Micrographs (SEM)

From the SEM micrographs (Fig. 3), DMZ crystals are irregular blocks with rough surface (Fig. 3a), while SAC crystals are irregular flakes with overlapping arrangement (Fig. 3b). DMZ-SAC crystals are well-formed rods (Fig. 3c).

Table 1. Crystallographic data for DMZ-SAC

	DMZ-SAC
Formula	$C_{12}H_{12}N_4O_5S$
CCDC no.	2063120
Formula weight	324.32
T/K	150
Wavelength/Å	1.54184
Crystal system	Monoclinic
Space group	$P2_1/n$
a / Å	6.8068 (1)
b / Å	7.9890 (2)
c / Å	25.3855 (4)
α /°	90
β /°	96.693 (2)
γ /°	90
V / Å^3	1371.04 (5)
Z	4
D_x/g cm^{-3}	1.571
R_{int}	0.0325
T_{min}	0.41322
T_{max}	1.00000
h, k,l_{max}	7,10,32
Mu (mm^{-1})	2.412
F000	672.0
θ_{max}	78.5810
GooF	1.051
R_1, wR_2 [I ≥ 4σ(I)][a]	0.0425,0.1113
R_1,wR_2[all data][b]	0.0443,0.1113

[a] $R_1=\Sigma\ |F_o| - |Fc|\ /\Sigma|F_o|$·[b] $wR_2 = [\Sigma[w(F_o^2 - Fc^2)^2]/\Sigma w(F_o^2)^2]^{1/2}$, $w = 1/[\sigma^2 (F_o)^2 + (aP)^2 + bP]$, where $P = [(F_o^2) + 2F_c^2]/3$.

FT-IR spectroscopy

The FT-IR spectrum of DMZ shows characteristic absorption band at 1182.74 cm^{-1}, which is assigned to C=N stretching, while that of SAC shows the N-H stretching band at 3401.77 cm^{-1} (Fig. 4). The C=N and N-H stretching bands in DMZ-SAC appear at 1178.91 cm^{-1} and 3448.43 cm^{-1}, respectively (Fig. 4). The shift in characteristic bands of these functional groups is consistent with the hydrogen bonding interaction between C=N of DMZ and N-H of SAC observed in the crystal structure of DMZ-SAC (Fig. 2a).

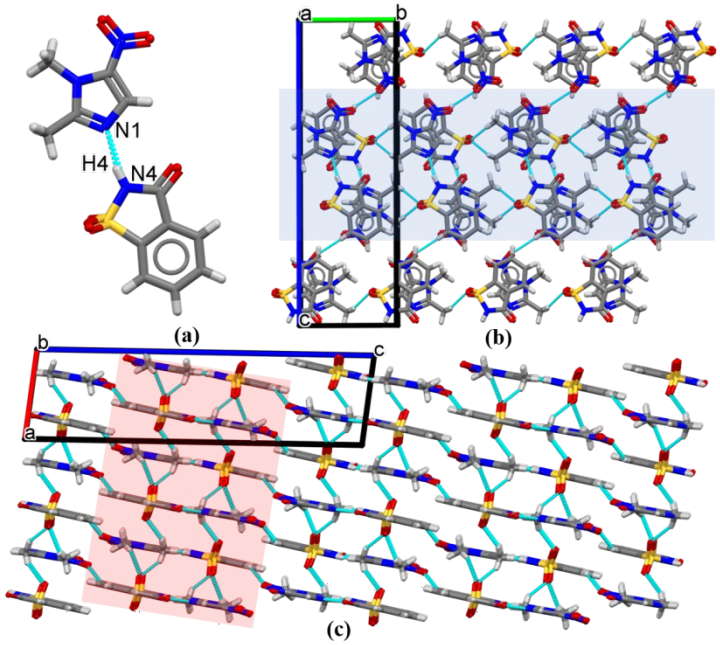

Fig. 2. (a) The asymmetric unit, (b) crystal structure viewed along the *a*-axis and (c) *b* axis. Parallel columns and a 2D layer are shaded in blue and red, respectively.

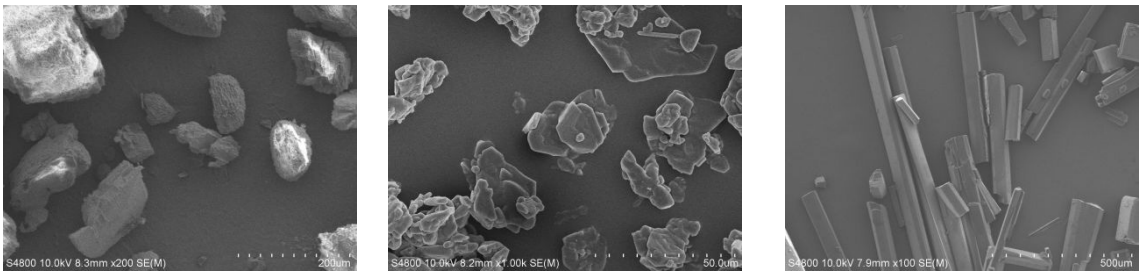

a b c

Fig. 3. SEM images of (a) DMZ, (b) SAC, and (c) DMZ-SAC

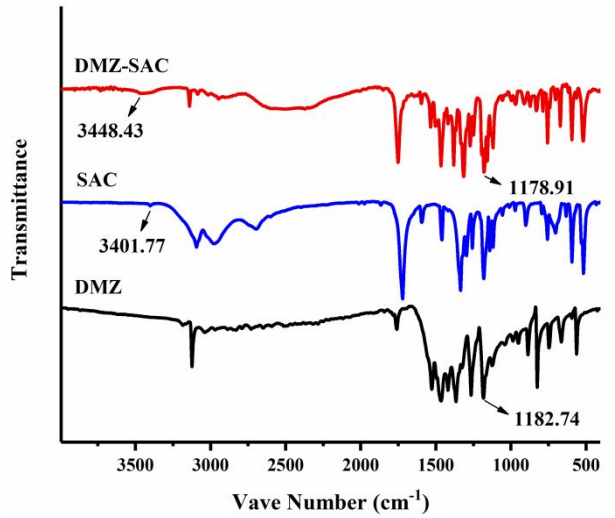

Fig. 4. FTIR spectra of DMZ, SAC and DMZ-SAC

Thermal Analysis

The DSC thermogram of DMZ shows an endotherm with an onset temperature of 138.7 °C (Fig. 5a). The endotherm corresponds to melting accompanied by evaporation of the melt since the sample mass reaches zero at approximately 200 °C (Fig. 5a). The thermal behavior of SAC is similar to that of DMZ except the onset temperature of the simultaneous melting and evaporation (227.5 °C) events is higher than that of DMZ (Fig. 5a, b), which are in agreement with reported thermal behavior of SAC.[35] The DSC thermogram of DMZ-SAC shows an endotherm with an onset temperature of 154.9 °C, followed by a broad exotherm up to 270 °C. The endotherm does not correspond to melting as the originally transparent DMZ-SAC crystals darkened at 125 °C without any sign of melting, as shown by the HSM experiment (Fig. 6). No weight loss of DMZ-SAC up to 150 °C was indicated by TGA. Hence, we attribute the endotherm to the solid-state dissociation of DMZ-SAC crystals. The broad exothermic event corresponds to gradual weight loss registered by TGA (Fig. 5c) and visually observed sublimation by HSM (Fig. 6). The mass loss of ~ 35% up to 220 °C likely corresponds to the loss of DMZ (theoretical

content is 43.5%). Subsequent weight loss is attributed to the loss of remaining DMZ and SAC.

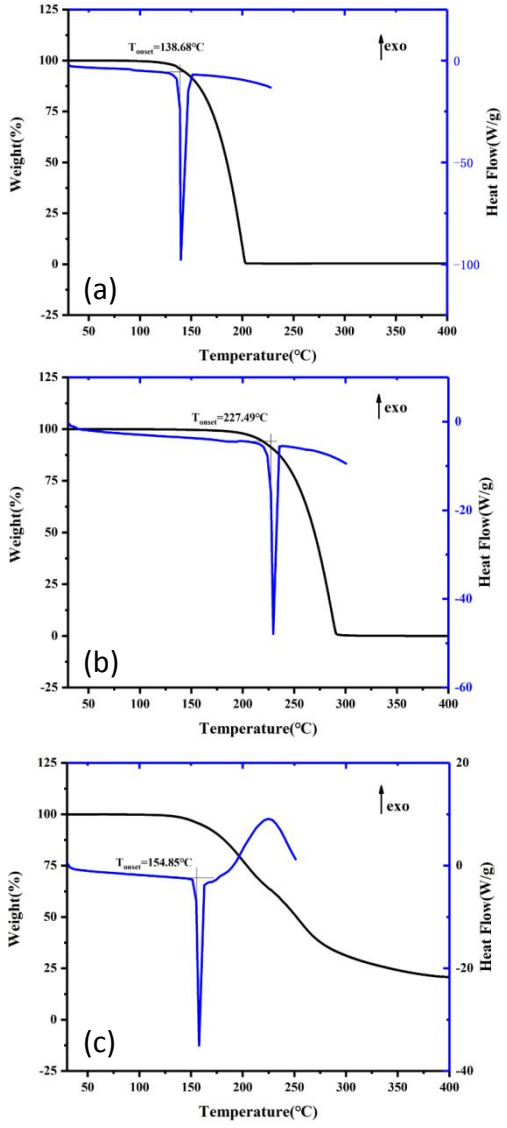

Fig. 5. TGA and DSC thermograms of (a) DMZ, (b) SAC and (c) DMZ-SAC

Photostability

To photo-stability experiments revealed significantly improved stability of DMZ-SAC over DMZ. For pure DMZ, only 80.38% of DMZ remained after 7 d. In contrast, 98.95% of DMZ in DMZ-SAC remained after 7 d (Fig. 7). The degradation in DMZ was accompanied by a pronounced color change, where the originally white powder changed to light green powder with increasing intensity over time (Fig. 8). No color change was observed in DMZ-SAC. Photo-degradation of DMZ was also observed in the 1:1 mole physical mixture with SAC. Thus, cocrystallization with SAC significantly stabilized DMZ, which is similar to the stabilization of nitrofurantoin and Vitamin K3 against photo-degradation by cocrystallization. [36, 37]

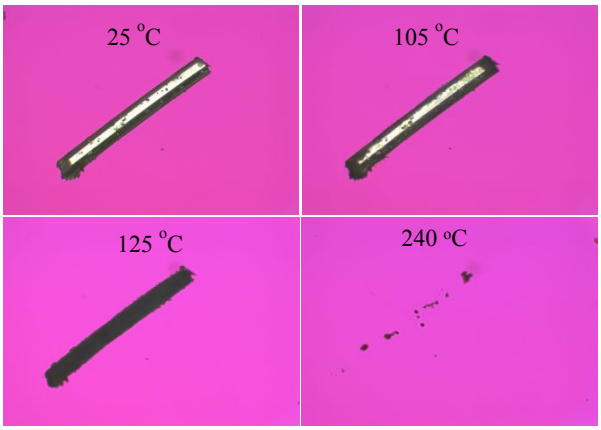

Fig. 6. Thermal behaviors of DMZ-SAC observed under a hot stage microscope

Mechanism of stabilization

To understand the molecular origin of the enhanced photostability of DMZ-SAC, the molecular conformation and intermolecular interaction strength of DMZ were analyzed. As a rigid molecule, the conformation of DMZ remains essentially unchanged in the commercial anhydrous form DMZ (CSD refcode: JIZJIL) and DMZ-SAC (Fig. 9a), with the calculated root-mean-square deviation between atomic positions of only 0.059. However, intermolecular interaction strength of DMZ in the two crystal forms are significantly different. In DMZ crystal, each DMZ molecule interacts with four neighboring DMZ molecules *via* C-H···N (D···A=3.392 Å) and C-H···O=N (D···A=3.482 Å) hydrogen bonds (Fig 9b). In comparison, each DMZ interacts with adjacent SAC molecules through N-H···N (D···A=2.739 Å) and C-H···O=N (D···A=3.214 Å and 3.478 Å) hydrogen bonds in DMZ-SAC (Fig 9c). The calculated total intermolecular interaction strength of DMZ in the DMZ crystal (-190.4 KJ/mol) is weaker than that of the cocrystal form (-203.3 KJ/mol). Detailed intermolecular interaction energies are summarized in Table S1. Therefore, the improved photostability of DMZ-SAC is attributed to the stronger intermolecular interactions rather than conformational differences. Importantly, each nitro group of DMZ only forms one weak C-H···O hydrogen bond with a neighboring molecules in DMZ (Fig. 9b), but two weak C-H···O hydrogen bonds with neighboring SAC molecules in DMZ-SAC (Fig. 9c). Thus, photo-degradation reaction of the nitro group in the cocrystal requires overcoming a larger energy barrier than that in DMZ.

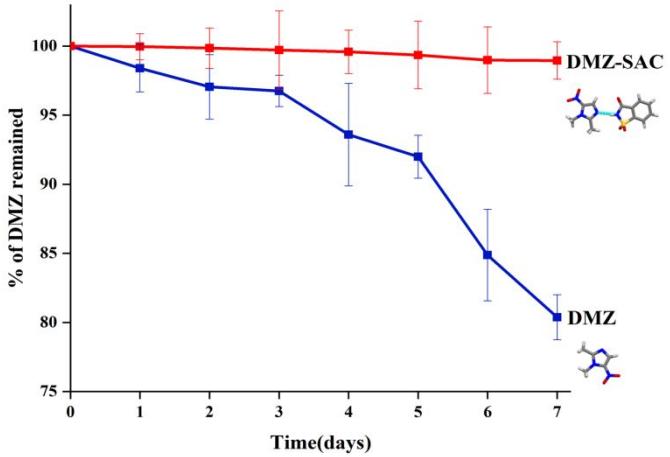

Fig. 7. Comparison of DMZ assay values for pure DMZ powder and DMZ-SAC after an illumination of 4500 lux for 7 days

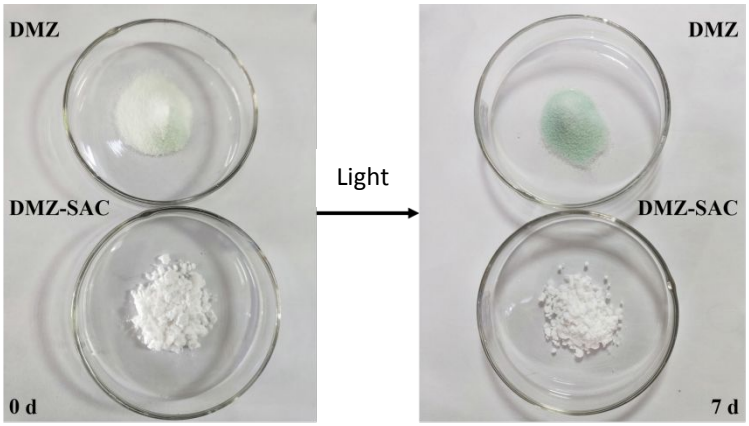

Fig. 8. Color change of DMZ upon exposure to light for 7 days. No color change ws observed for DMZ-SAC under the same conditions.

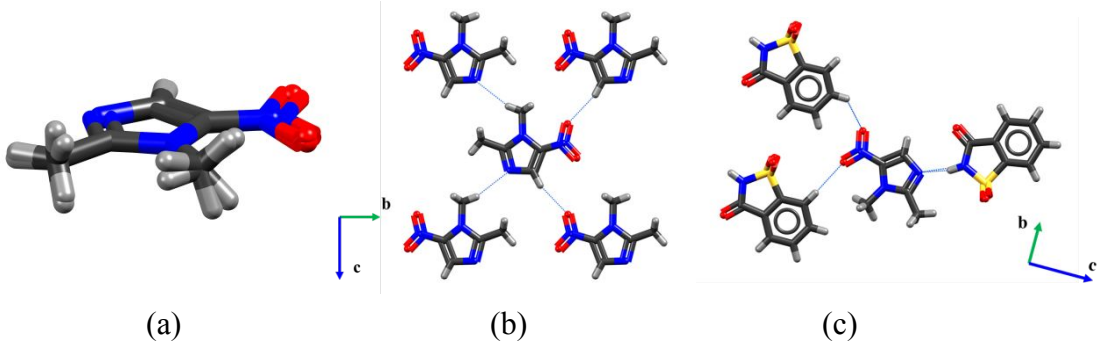

Fig. 9. (a) Overlaid two DMZ molecules in DMZ and DMZ-SAC, and main intermolecular interactions in (b) DMZ anhydrous and (c) DMZ-SAC.

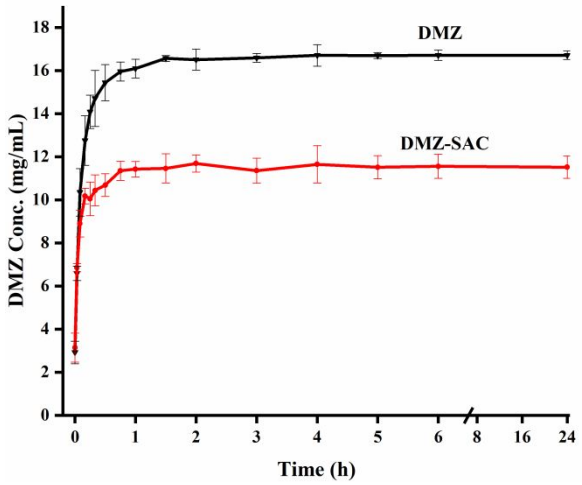

Fig. 10. Powder dissolution profiles of DMZ-SAC and DMZ in water at 37 °C.

Dissolution studies

Given the importance of solubility and dissolution rate in drug delivery,[38] the impact of cocrystallization on powder dissolution rate of DMZ was also assessed in water. Both crystals reached a plateau concentration in about 2 hr (Fig. 10). DMZ-SAC remained phase pure during the course of dissolution as confirmed by PXRD of the isolated solid at the end of the experiment (Fig. S1). Since the plateau concentration corresponds to solubility of each solid form, DMZ (16.5 mg/mL) is more soluble than DMZ-SAC (11.5 mg/mL) in water at 37 °C. The lower solubility of the DMZ-SAC cocrystal is consistent with its higher thermal stability than DMZ (Fig. 5).[39] Additionally, the relatively lower aqueous solubility of SAC (4 mg/mL)[40] also contributes to the lower solubility of DMZ-SAC as the solubility of cocrystals generally positively correlates with the solubility of coformers for a given API.[41, 42,43] The lower solubility of DMZ-SAC does not present a problem in DMZ delivery since a dose up to 2.875 g can be completely dissolved in 250 mL water.

Conclusions

The pharmaceutical cocrystal of the antibacterial veterinary drug, DMZ, with SAC were successfully prepared and its solid-state properties have been characterized. The DMZ-SAC cocrystal showed strikingly better photostability compared to DMZ, which is attributed to the stronger interaction energies of DMZ in the cocrystal. Thus, this cocrystal has the potential to enable the development of a more stable tablet formulation of dimetronidazole.

Author Contributions

Xinghui Hao and Jinhui Li for the investigation of the project, Chenguang Wang for the data curation, Xinghua Zhao for funding acquisition, Xin He for original draft writing, Xin He and Changquan Calvin Sun for funding acquisition, data review, and revising the manuscript.

Conflicts of interest

There are no conflicts to declare.

Acknowledgements

This work was financially supported by Key R&D Program of Hebei Province (No. 19227505D) and Educational Commission of Hebei Province of China (ZD2019109). We thank the Minnesota Supercomputing Institute [44] at the University of Minnesota for providing the resources that contributed to the research results reported within this paper (http://www.msi.umn.edu). CCS thanks the National Science Foundation for support through the Industry University Collaborative Research Center grant IIP-2137264, Center for Integrated Materials Science and Engineering of Pharmaceutical Products (CIMSEPP).

Notes and References

1. M. Keerthi, M. Akilarasan, S. M. Chen, S. Kogularasu, M. Govindasamy, V. Mani, M. A. Ali, F. M. A. Al-Hemaid and M. S. Elshikh, *J. Electrochem. Soc.*, 2018, **165**, B27-B33.
2. T. L. Fodey, L. Connolly, S. R. H. Crooks, P. Delahaut and C. T. Elliott, *Anal. Chim. Acta*, 2003, **483**, 193-200.
3. M. J. Parnell, *Pestic. Sci.*, 1973, **4**, 643-646.
4. P. J. Quinlivan and R. K. Upmacis, *Acta Crystallogr., Sect. E. Crystallogr. Commun.*, 2016, **72**, 1633-1636.
5. L. H. Stanker, C. Mckeown, B. E. Watkins, M. Vanderlaan, R. Ellis and J. Rajan, *J. Agric. Food Chem.*, 1993, **41**, 1332-1336.
6. A. Salahuddin, S. M. Agarwal, F. Avecilla and A. Azam, *Bioorg. Med. Chem. Lett.*, 2012, **22**, 5694-5699.
7. M. Sarker, S. Shin and S. H. Jhung, *J. Hazard. Mater.*, 2019, **378**, 120761.
8. J. Rivera-Utrilla, G. Prados-Joya, M. Sanchez-Polo, M. A. Ferro-Garcia and I. Bautista-Toledo, *J. Hazard. Mater.*, 2009, **170**, 298-305.
9. Chemical Book, *https://www.chemicalbook.com/ProductIndex_EN.aspx*.
10. P. W. Seo, N. A. Khan and S. H. Jhung, *Chem. Eng. J.*, 2017, **315**, 92-100.
11. B. Marciniec, A. Bugaj and W. Kędziora, *Pharmazie*, 1997, **52**, 220-223.
12. R. F. Dantas, O. Rossiter, A. K. R. Teixeira, A. S. M. Simões and V. L. da Silva, *Chem. Eng. J.*, 2010, **158**, 143-147.

13. B. Wu, T. Zhang, J. Li, Y. Ye and H. Chen, *Water Sci. Technol.*, 2012, **66**, 735-740.
14. O. E. Fandiño, L. Reviglio, Y. G. Linck, G. A. Monti, M. M. Marcos Valdez, S. N. Faudone, M. R. Caira and N. R. Sperandeo, *Cryst. Growth Des.*, 2020, **20**, 2930-2942.
15. X.-L. Dai, C. Wu, J.-H. Li, L.-C. Liu, X. He, T.-B. Lu and J.-M. Chen, *CrystEngComm*, 2020, **22**, 3670-3682.
16. J.-R. Wang, C. Zhou, X. Yu and X. Mei, *Chem Commun (Camb)*, 2014, **50**, 855-858.
17. S. Aitipamula, V. R. Vangala, P. S. Chow and R. B. H. Tan, *Cryst. Growth Des.*, 2012, **12**, 5858-5863.
18. S. Mittapalli, M. K. C. Mannava, U. B. R. Khandavilli, S. Allu and A. Nangia, *Cryst. Growth Des.*, 2015, **15**, 2493-2504.
19. O. O. Abosede, A. T. Gordon, T. O. Dembaremba, C. M. A. Lorentino, H. F. Frota, A. L. S. Santos, E. C. Hosten and A. S. Ogunlaja, *Cryst. Growth Des.*, 2020, **20**, 3510-3522.
20. H. Yamashita and C. C. Sun, *Pharm. Res.*, 2018, **35**, 4.
21. F. Liu, F.-B. Jiang, Y.-t. Li, R.-M. Liu, Z.-Y. Wu and C.-W. Yan, *Drug Dev. Ind. Pharm.*, 2020, **46**, 988-995.
22. C. Wang, Q. Tong, X. Hou, S. Hu, J. Fang and C. C. Sun, *Cryst. Growth Des.*, 2016, **16**, 5030-5039.
23. X. Zhao, Q. Li, C. Wang, S. Hu, X. He and C. C. Sun, *Int. J. Pharm.*, 2020, **577**, 119089.
24. S. Allu, G. Bolla, S. Tothadi and A. K. Nangia, *Cryst. Growth Des.*, 2020, **20**, 793-803.
25. Q. Yu, Z. Yan, J. Bao, J.-R. Wang and X. Mei, *Chem. Commun.*, 2017, **53**, 12266-12269.
26. S. K. Pagire, C. C. Seaton and A. Paradkar, *Cryst. Growth Des.*, 2020, **20**, 4839-4844.
27. S. Hu, C. Wang, X. He and C. C. Sun, *Cryst. Growth Des.*, 2020, **20**, 2057-2063.
28. C. Wang, S. R. Perumalla, R. Lu, J. Fang and C. C. Sun, *Cryst. Growth Des.*, 2016, **16**, 933-939.
29. P. Sanphui, S. S. Kumar and A. Nangia, *Cryst. Growth Des.*, 2012, **12**, 4588-4599.
30. A. J. Smith, P. Kavuru, K. K. Arora, S. Kesani, J. Tan, M. J. Zaworotko and R. D. Shytle, *Mol. Pharmaceutics*, 2013, **10**, 2948-2961.
31. M. J. Turner, S. Grabowsky, D. Jayatilaka and M. A. Spackman, *J Phys Chem Lett*, 2014, **5**, 4249-4255.
32. Y. Guo, M. K. Mishra, C. Wang and C. C. Sun, *Mol. Pharmaceutics*, 2020, **17**, 579-587.
33. C. Wang and C. C. Sun, *Mol. Pharmaceutics*, 2019, **16**, 1732-1741.
34. H. Chen, H. Xu, C. Wang, H. Kang, C. L. Haynes, M. K. Mahanthappa and C. C. Sun, *Cryst. Growth Des.*, 2020, **20**, 6752-6762.
35. S. Basavoju, D. Bostrom and S. P. Velaga, *Pharm. Res.*, 2008, **25**, 530-541.
36. V. R. Vangala, P. S. Chow and R. B. H. Tan, *Cryst. Growth Des.*, 2012, **12**, 5925-5938.
37. B. Zhu, J.-R. Wang, Q. Zhang and X. Mei, *Cryst. Growth Des.*, 2015, **16**, 483-492.
38. Y. Yan, J.-M. Chen and T.-B. Lu, *CrystEngComm*, 2015, **17**, 612-620.
39. S. Modani, A. Gunnam, B. Yadav, A. K. Nangia and N. R. Shastri, *Cryst. Growth Des.*, 2020, **20**, 3577-3583.
40. A. John and I. J. Motoi, *J Mutation Research*, 1986, **163**, 63-73.
41. R. Thakuria, A. Delori, W. Jones, M. P. Lipert, L. Roy and N. Rodriguez-Hornedo, *Int. J. Pharm.*, 2013, **453**, 101-125.
42. X.-L. Dai, J.-M. Chen and T.-B. Lu, *CrystEngComm*, 2018, **20**, 5292-5316.
43. O. H. Azeez, S. Y. Alkass and D. S. Persike, *Medicina*, 2019, **55**, 681.
44. F. Zamani-Garmsiri, S. M. R. Hashemnia, M. Shabani, M. Bagherieh, S. Emamgholipour and R. Meshkani, *J Nutr Biochem*, 2021, **87**, 108505.

